Indoor air treatment of refrigerated food chambers with synergetic association between cold plasma and photocatalysis: Process performance and photocatalytic poisoning

Tahar Zadi, Mohamed Azizi, Noureddine Nasrallah, Abdelkrim Bouzaza, Rachida Maachi, Dominique Wolbert, Sami Rtimi, Aymen Amin Assadi

Indoor air treatment of refrigerated food chambers with synergetic association between cold plasma and photocatalysis: process performance and photocatalytic poisoning

Tahar Zadi[1,2], Mohamed Azizi[3,4], Noureddine Nasrallah[1], Abdelkrim Bouzaza[2], Rachida Maachi[1], Dominique Wolbert[2], Sami Rtimi[5]*, Aymen Amin Assadi[2]**

[1] Laboratory of Reaction Engineering, Faculty of Mechanical Engineering and Process Engineering, USTHB, BP 32, Algiers, Algeria

[2]Unir, ENSCR-11, allée de Beaulieu, CS508307-35708 Rennes, France.

[3]Faculty of Science and Arts-Qilwah, 65941, Albaha University, Saoudi Arabia.

[4]Centre de Recherche et de Technologies des Eaux, CERTE, Laboratory of Nature Water Treatment (LabTEN), BP 273, Soliman 8020, Tunisia.

[5]Swiss Federal Institute of Technology (EPFL), EPFL-SB-ISIC-GPAO, 1015 Lausanne, Switzerland

* Corresponding authors. Tel.: +33 2 23238056; fax: +33 2 23238120.

E-mail addresses: aymen.assadi@ensc-rennes.fr (A.A. Assadi) sami.rtimi@epfl.ch (S. Rtimi).

Abstract

The purpose of this study is to evaluate the efficiency of non-thermal plasma (NTP) and heterogeneous photocatalytic processes for indoor air treatment of refrigerated food chambers. Propionic acid and benzene were chosen as target pollutants to simulate odors inside a fridge. Firstly, the microstructure of the used catalyst was investigated by transmission electron microscopy (TEM). The influence of operating parameters such as pollutant concentration, type of system (mono-compound or bi-compound system), duration of photocatalytic degradation and relative humidity in the indoor air were investigated. Our findings show a synergetic effect between NTP and photocatalysis for malodors removal. Additionally, the mineralization of pollutant is directly controlled by the amount of ozone produced by the plasma discharge then it decomposes on the TiO_2-based catalytic surface. Our results highlight also the key role of the generated reactive oxygen species (hydroxyl radials and atomic oxygen) in (i) propionic acid and benzene removal, (ii) selectivity of CO_2 and CO, (iii) by-products formation such as ozone

formation. Moreover, the recovery of the initial photocatalytic activity was explored in details. A significant poisoning occurred when photocatalysis was carried out alone for the degradation of propionic acid and benzene. Results confirm that NTP plasma enhanced the photocatalytic activity. We also showed the effect of NTP plasma on the regeneration of the photocatalytic surface.

Keywords: indoor air; mineralization; photocatalytic poisoning; synergistic effect, combination NTP plasma/photocatalysis.

1. Introduction

In recent decades, odors have become important elements of air pollution [1]. Odorants are defined as air pollution that stimulates the nerve cells of the olfactory epithelium. While odor is a term used compared to mixtures of odor-damaging substances, which are atmospheric pollutants [2,3]. Indoor air pollution is now considered among the top five environmental risks to public health according to the environmental protection agency (EPA), which declared the air to be two to five times more polluted indoors than outdoors [3]. The smell of agricultural locals and agro-food and refrigerator facilities is linked to the emission of several hundred different substances in the air, in particular carboxylic acids, ammonia, benzene, phenols, aldehydes and others [4-8]. Their emission concentrations are not yet strictly controlled in many countries [9,10]. Odor compounds have a generally unpleasant smell and are well known to have a harmful effect on health with the associated consequences. Odors are formed in the fermentation process when litter, urine, feces and food remain decomposed, as well as during breathing, digestion and evaporation of animal skin [11-13]. Several studies have shown that long-term exposure to odors negatively affects people's mood and behavior. It has been found that they can cause many ailments, such as insomnia, stress, listlessness, irritability, depression, headaches, coughing, runny nose and cramps in the mouth and allergic reactions [11, 12]. These

compounds are dangerous at high concentrations. Propionic Acid (PPA, $C_3H_6O_2$), classified as volatile fatty acid (VFA), is usually produced in the early stages of anaerobic degradation of the organic substance, acids are more or less irritating and corrosive [14,15]. Of all the gaseous pollutants, Benzene (Benz, C_6H_6) may be one of the most hazardous of the volatiles organics compounds (VOCs) because of its high toxicity, confirmed carcinogenicity, and environmental persistence [16], a highly stable chemical used widely in the industry and indoor decoration materials, was indicated as a common volatile air pollutant. Recent works demonstrated that the photocatalytic destruction of C_6H_6 can be readily achieved on some hydroxides, the abatement of C_6H_6 has been hardly achieved on oxide semiconductors [17,18].

To date, various VOCs treatment techniques have been developed and used such as combustion, absorption, adsorption, membrane filtration, plasma and photocatalytic oxidation (PCO) [17]. On several occasions, activated carbon adsorption was commonly recommended for indoor air purification because of its thermal desorption reuse and ability to remove low level VOCs. However, the adsorption essentially relies just on the transfer of chemical components between two phases without destruction. Developing a more effective tool to eliminate major odors in our living environment, we explored the feasibility of a PCO-based technique (e.g. TiO_2, ZnO, MoS_2/g-C_3N_4 nanocomposites) for the environmental cleansing of nuisances, especially with regard to nitric oxide (NO) [19] and food odorants [5,19,20]. The PCO method has demonstrated its ability to convert a wide range of air pollutants into harmless compounds (H_2O and CO_2 as end products) [21, 22]. In recent years, titanium dioxide (TiO_2) has been widely used because of its potential to degrade a wide range of VOCs [23].To explore the applicability of the PCO approach, we investigated the deodorization efficiency with respect to both odors. The results of this study will thus provide valuable information for practical use of the photocatalytic elimination of different odors from indoor environment (houses, hospitals, industry).

Sang-Hee et al. [5] studied the volatile odorants that can be released from non-decayed foods. They used 10 types of food samples (raw beef, raw chicken, spam, onion, tomato, strawberry, boiled egg, cod fish, mackerel, and French cheese). The identification of the malodors revealed relatively high concentrations of propionic acid (PPA) and benzene (BENZ).

An extreme environment is defined as a set of values/conditions above which a material (in our case the photocatalyst) may be considered subject to significant performance alterations. Extreme environment refers to accident environments or abnormal operational conditions of temperature, pressure, pH, composition… In our study, we investigate the photocatalytic and non-thermal plasma performance under low temperature as in refrigerated rooms.

In the present study, PPA and BENZ were chosen as target pollutant in a refrigerated room. Here, the coupling of non-thermal plasma (NTP) with photocatalytic oxidation is presented for the elimination of PPA and BENZ in a food-refrigerated chamber. The optimization of the used processes for the indoor air treatment as well as the catalyst poisoning and its regeneration are studied in detail. The novelty of this study is to investigate the synergetic effect between non-thermal plasma and heterogeneous photocatalysis for PPA+BENZ mixture removal in extreme environment (refrigerated food chambers). During the elimination, the contribution of each process in the pollutants' removal has been discussed.

2. Experimental and measurement

2.1. Pilot system and setup details

The pilot designed to study the coupling between photocatalysis (SiO_2-TiO_2+UV) and dielectric barrier discharge (DBD) plasma is shown in Figure 1. The plasma emits in the UV wavelengths as it was studied in details in a previous work [24]. The set-up includes an effluent preparation system, a cylindrical reactor that can operate either for the PCO and/or to generate the NTP, or by coupling the two processes. It was previously reported that plasma-processes generate

ozone; this O_3 generation is also investigated. The airflow rate is controlled by a flowmeter (Bronkhorst In-Flow type E-700) coupled to a precision valve. To vary the relative humidity (RH) the main air flow is generated by two ways. When (RH < 5%), we use the internal compressed air network. To obtain a RH ranging from 25 to 90%, a centrifugal pump is used with the ambient air. To change the RH, a fraction of the intake air passes through a column filled with Raschig rings. The pollutants, propionic acid (PPA) and benzene (BENZ), in the liquid state, are injected continuously into a stream of air by means of a syringe-pump syringe system (Kd Scientific Model 100), through a septum. A heating tape was wrapped around the pipe of the injection zones to ensure good evaporation of each pollutant.

The cylindrical NTP/SiO_2-TiO_2+UV reactor is shown in Figure 2. It consists of two concentric Pyrex glass tubes with internal diameters of 58 mm (inner cylinder) and 76 mm (outer cylinder). The reactor can be fed either with a stream of air charged with a pure compound or with a binary mixture. Glass Fiber Tissue (GFT) was coated with SiO_2-TiO_2 used as the main photocatalytic material. The photocatalyst contains 6.5 g m^{-2} of colloidal silica, 6.5 g m^{-2} of titanium dioxide nanoparticles on the inorganic fibers. The coating process is based on the impregnation of the glass fibers with nanoparticles of SiO_2 and TiO_2 suspended in an aqueous solution using the size-press technique that was patented by Ahlstrom Research and Services (PC500 Millennium) [25]. Experiments were carried out in dynamic (non-steady) mode. This choice is justified by the non homogeneous distribution of VOC pollutants in a real setting (industry, hospitals, restaurants, houses). It is worth to mention at this level that it is quite difficult to reach a steady-state condition because we are working with a Plug flow reactor. The air (air charged with VOC) is going through the reactor as a series of infinite thin coherent plugs. Each plug in the reactor shows a uniform composition, however, each plug has a different composition from the ones before and after it. It is worth to mention that as a plug flows through the reactor, the fluid

is assumed to be perfectly mixed in the radial direction but not in the axial direction (forwards or backwards).

Before starting the photocatalytic process, an adsorption phase (30 min) was carried out in order to reach quiet an equilibrium of adsorption/desorption. To estimate the adsorbed amount of pollutant during this period (assuming that all the catalytic active sites are free), we should take into consideration the amount of TiO2 supported on the glass fiber and the flow rate. Using this assumption, we find that 10 mg of pollutant can adsorb on 1g of TiO_2.

To visualize the microstructure of the prepared catalyst, the coated glass fibers were embedded in epoxy polymer then cut with ultra-microtome into thin layers with thickness of 80-100 nm. These layers were placed on TEM carbon grid. FEI Osiris microscope was used for imaging and operated at 200 kV, with spot size of 5, dwell time 50 μs and real time 600 s. X-ray diffraction (XRD) was operated on an X'Pert MPD PRO from PANalytical equipped with a secondary graphite monochromator and a PIXcel-1D detector operated in Bragg-Brentano geometry. Uncoated fiberglass fabrics were used as background.

A UVA lamp Philips CLEO performance 80W/10 model illuminated the photocatalytic material with an output intensity of $25W/m^2$.

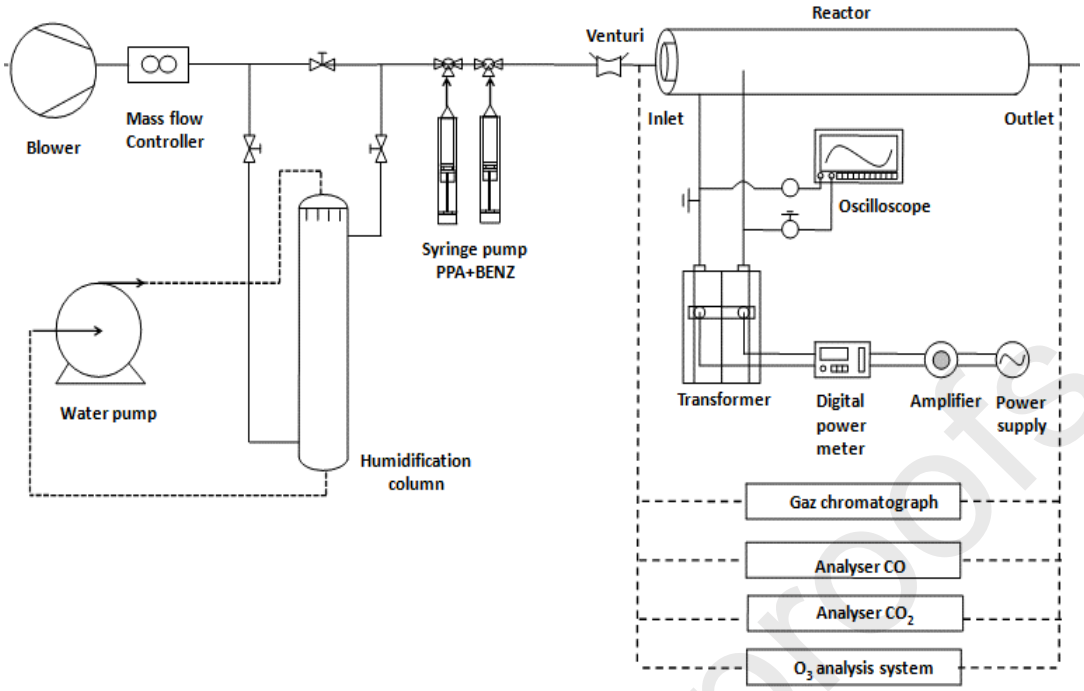

Figure 1. General Schematic view of the pilot system: photocatalysis and NTP.

To visualize and generate the plasma, a high voltage is applied by a generator (BFi OPTILAS) up to 10V as a sinusoidal waveform, and then this generator is connected with an amplifier (Model TREK PD06035) to reach 30 kV, coupled to a signal generator (reference BFI Optilas DS 335/1). A digital oscilloscope (Lecroy Wave Surfer 24 Xs, 200 MHz) allows visualizing the high voltage applied and the voltage across the capacity. The electrical system of the NTP reactor has been described in detail in our previous work [26].

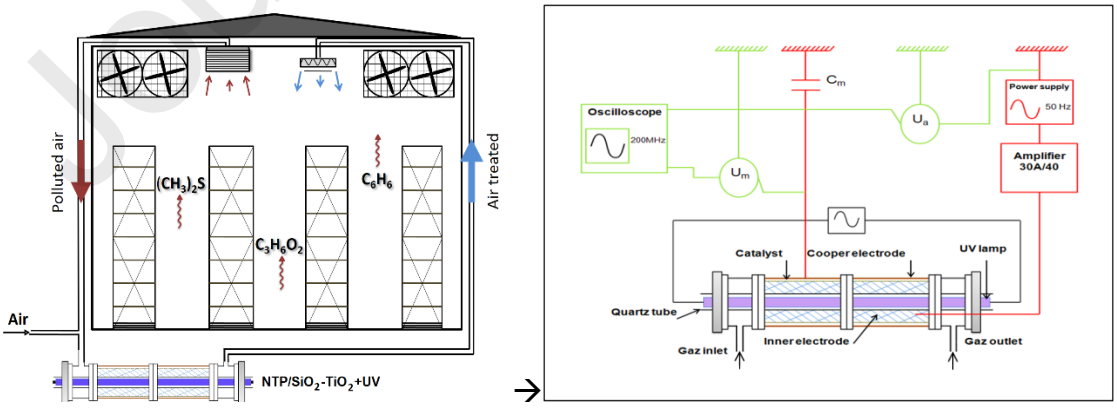

Figure 2. Schematic view of the annular reactor coupling photocatalysis and NTP for the treatment of the air in a refrigerated room.

2.2. Apparatus and Analysis

Samples of PPA and BENZ were manually collected with a 500 µL syringe. The concentrations were analyzed using a gas chromatography (Fisons GC 9000 series, Thermo Focus, USA) equipped with flame ionization detector (GC-FID). The FID-detector is powered by a mixture of air and hydrogen (H_2). Nitrogen (N_2) was used as a carrier gas. The CO_2 Analyzer is a MIR 9000 Environment SA multi-gas infrared analyzer using GFC (Gas Filters Correlation) technology used. The measurement of the amount of CO_2 formed during the pollutant treatment phase is performed online using a Fourier Transform Infrared Spectrophotometer (FTIR). For CO monitoring at the output of the pilot reactor, a NO/CO ZRE gas analyzer (Fuji Electric France S.A.S) was connected. Ozone was generated by the plasma during the treatment of gaseous effluent and was analyzed by colorimetric assay after bubbling [27]. At the outlet air flow, a flow rate of 242 L h^{-1} of the gaseous phase is sent by a membrane pump (KNF lab N86k18) to a 500 mL volume bubbler, which contains a solution of potassium iodide (KI) at 10^{-2} M. The color of the solution turned yellowish due to the presence of O_3 leading to the oxidation of I^- to I_2. I_2 is then titrated until discoloration with a solution of $Na_2S_2O_3$ 10^{-3} M. This titration is carried out in acidic medium (H_2SO_4).

To evaluate the process performance, the Removal Efficiency (RE) was estimated using Eq.1:

$$RE\ (\%) = ([C]_{inlet} - [C]_{outlet}) \times 100 / [C]_{inlet} \qquad \text{Eq.1}$$

Inlet $[C]_{inlet}$ and outlet $[C]_{outlet}$ concentrations of pollutants in (mmoL m^{-3}) respectively.

The Rate of Synergy (RS) between the two processes was calculated using the following expression:

$$RS = RE_{combined\ process}/(RE_{plasma} + RE_{photocatalysis}) \quad \text{Eq.2}$$

The carbon dioxide selectivity (SCO_2) and the carbon monoxide selectivity (SCO) were determined using the following equations:

$$SCO_2(\%) = ([CO_2]_{outlet} - [CO_2]_{inlet}) \times 10^4 / (n_{C,VOC} \times RE \times [C]_{inlet}) \quad \text{Eq.3}$$

$$SCO\ (\%) = ([CO]_{outlet} - [CO]_{inlet}) \times 10^4 / (n_{C,VOC} \times RE \times [C]_{inlet}) \quad \text{Eq.4}$$

Where [C] is the concentration of PPA and/or BENZ in mmoL m^{-3}, $n_{C,VOC}$ represents the number of carbon in the molecules (3 for PPA and 6 for BENZ).

3. RESULTS AND DISCUSSION

3.1. Microstructure of the catalyst and surface atomic composition

Figure 3 shows the HAADF distribution of the SiO_2-TiO_2 coating on the fiber glass fabrics. Figure 3 shows that the coating is well distributed along the glass fibers. The Si/Ti ratio of 1 (see experimental section) allows the SiO_2 to play the role of a binder for a homogeneous distribution of TiO_2. The binder tightly bonds the TiO_2 particles leading to the formation of a compact layer/coating. The SiO_2 binder can also help to alleviate the possible stress of TiO_2 nanoparticles subsequent to the volume change during the size-press preparation. The SiO_2 encompass TiO_2 leading to the formation of TiO_2-ilands. The glass fiber support was used to avoid the fabric burns when exposed to the plasma discharge zone. Indeed, this support resists perfectly to the electric shock of the plasma generated on the surface. Figure 3b shows the crystallinity of the used photocatalyst during the course of this study. The TiO_2 present on the fiberglass is predominantly Anatase. The TiO_2 aggregates, as shown in Figure 3a, are mainly formed of crystallites of 8-12 nm. The aggregates size are 0.5-1.5 µm as shown in the elements mapping in Figure 3a.

a)

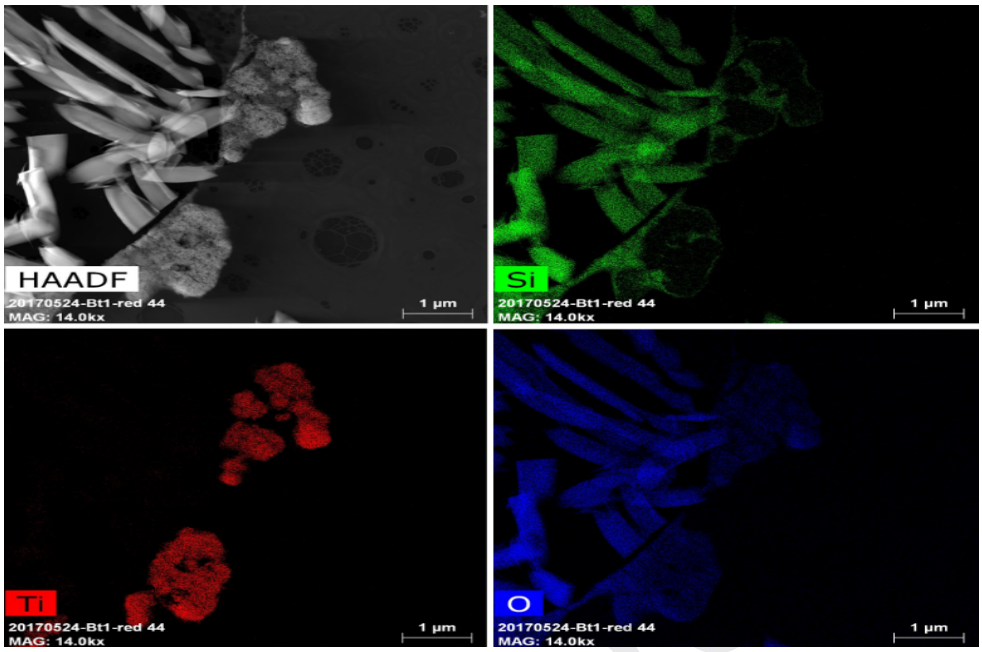

b)

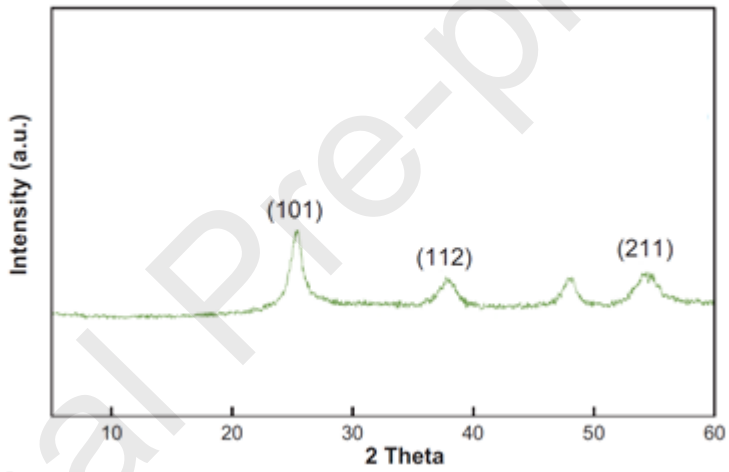

Figure 3. a) HAADF coating distribution and elements mapping of the photocatalyst used in the present study, b) XRD diffractogram of the used photocatalyst.

The total elimination of PPA alone (100% PPA), benzene alone (100% BNEZ) and their mixture (50% PPA + 50% BENZ) in a continuous annular reactor (non-steady condition) were investigated. First, the photocatalytic oxidation (SiO_2-TiO_2-UV) of the two odor pollutants was performed. Afterward, NTP performance for the elimination of PPA and BENZ was studied. The combination of photocatalysis and plasma (NTP / SiO_2-TiO_2-UV) for both pollutants removal in the same reactor was subsequently studied.

3.2. Study of component degradation with photocatalysis alone

The removal of different concentrations of PPA and BENZ has been studied. The variation of the effect of the inlet flow and the relative humidity (RH) were also investigated. Odor inlet concentrations ranged from 0.068 to 0.405 mmoL m^{-3} and effluent flow rates were in the range of 2-6 m^3 h^{-1} and Relative Humidity from 5 to 90%.

3.2.1. Effect of residence time and inlet concentrations on PPA degradation

Figure 4 shows the removal efficiency of PPA by varying the inlet concentration. It is readily seen from Figure 4 that the concentration effect shows that the increase of the inlet concentration led to the decrease of the removal efficiency. At high concentration of PPA, the removal efficiency tends to be limited. This behavior could be explained by the occupation of the available active sites on the surface of the catalyst. Figure 4 shows also that the removal efficiency of PPA decreases with increasing flow rate. This can be attributed to the decrease in the residence/contact time between the pollutant and the actives sites on the surface of the catalyst such as hydroxyl radicals [28-30].

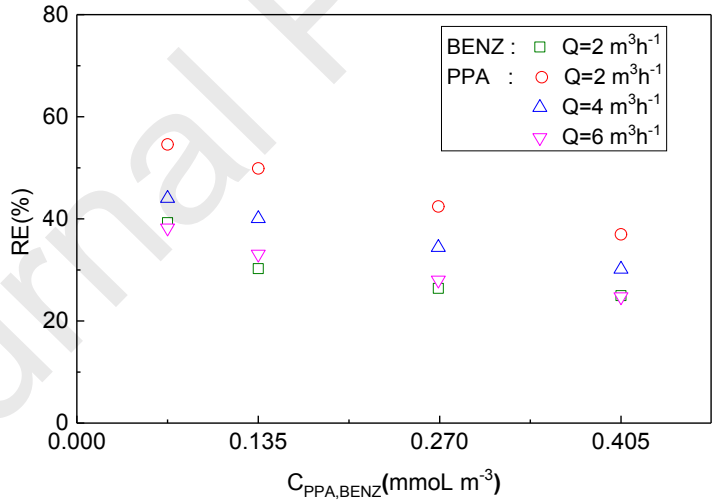

Figure 4. Influence of inlet concentration and flow rates with on the removal efficiency of PPA and BENZ by photocatalysis I= 20 W m^{-2}, T = 20 °C. Error bars: standard deviation (SD) (n= 5%)

3.2.2. Effects of inlet concentration and relative humidity for BENZ

Figure 5 shows the influence of inlet concentration at different RH on the RE with photocatalysis. The RH has been varied to get three scenarios/conditions: dry air of 5%, average humidity of 50% and high humidity of 90% at different inlet concentrations of BENZ. The obtained results (Figure 5) show that the presence of water molecules in the gaseous effluent improves the oxidation of BENZ. It seems that there is an optimum (RH =50%) where the RE is 25% and reaches a maximum of 40% at 0.0675 mmoL m-3 of BENZ. However, a slight increase in the RH allows the increase of the photo-generation of •OH as previously reported [31]. As •OH-radical is highly oxidative, the increase of its concentration will lead to an increase in the conversion rate of BENZ. Additionally, when the RH increases, the competitive effect of adsorption toward the TiO_2 active sites of the water becomes predominant [32]. Then the RH has a negative effect on BENZ oxidation performance resulting from strong competition between water molecules and the pollutant at catalyst sites. It is worth to mention at this level that with a flowrate of 2 $m^3 h^{-1}$, the pollutant residence time is of 2.7 s.

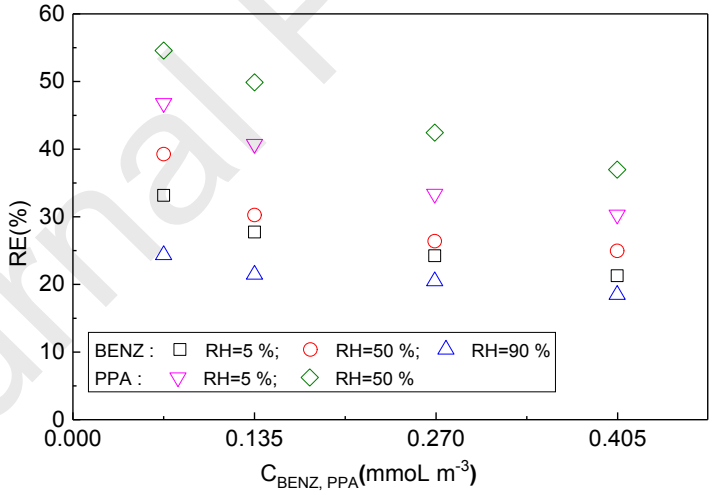

Figure 5. Influence of the inlet concentration to different RH on the RE of BENZ and PPA with photocatalysis: Q= 2 $m^3 h^{-1}$, I= 20 W m^{-2}, T = 20 °C. Error bars: SD (n= 5%)

3.3. Effect of the injected voltage during NTP process

In order to study the influence of the voltage injected by NTP alone on the degradation of the two pollutants, the reactor was powered with a gaseous effluent (100% PPA and 100% BENZ)

at a flowrate of 2 m^3 h^{-1} and at an equivalent concentration of 0.135 mmoL m^{-3}. Figure 6 shows the RE of PPA and BENZ as a function of the voltages injected into the reactor. The results obtained by applying plasma only show that the increase of the input voltages causes an increase in the RE. This can be attributed to the reactive species generated in the reaction medium. This will not be further discussed in the present study and more details can be found in the literature and in our previous publications [33-36].

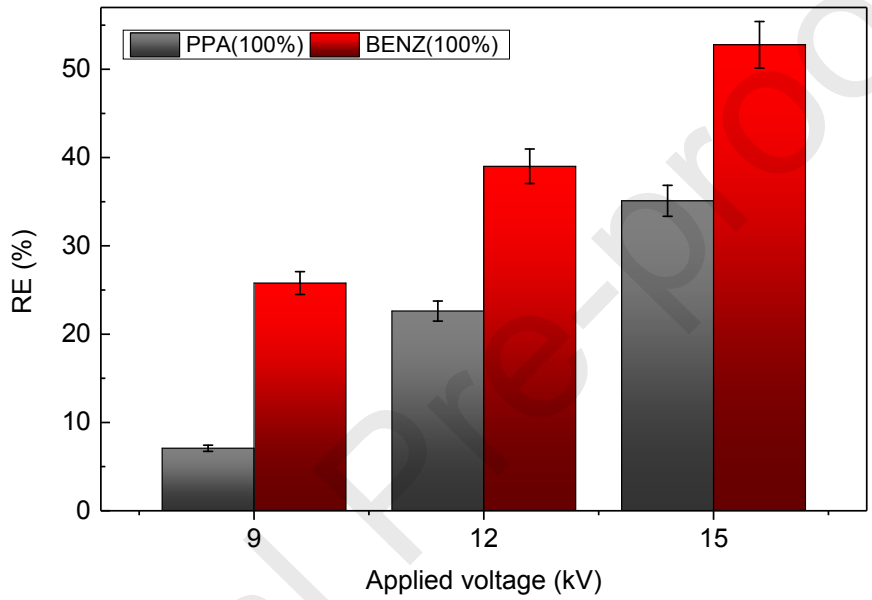

Figure 6. Evolution of the RE of PPA and BENZ at different values of high voltage during oxidation with the plasma process. [Mixture] = 0.135 mmoL m^{-3}, Q = 2 m^3 h^{-1}, HR = 50%, T = 20 °C. Error bars: SD (n= 5%)

3.4. Study of the removal of gas mixture system

3.4.1. Photocatalytic oxidation of the mixture PPA and BENZ

In order to compare the degradation efficiency of the pure and the mixture system of PPA and BENZ at the inlet gas, different pollutant(s) concentration(s) (between 0.067 and 0.405 mmol m^{-3}) were tested with a flow rate equal to 2 m^3 h^{-1} and 50% relative humidity. Figure 7 shows the RE for a pure and mixed system in the presence of the photocatalyst and the light source. When each pollutant has been tested alone, the removal efficiencies were 55% (PPA) and 40%

(BENZ). However, the removal efficiencies of the mixture were equal to 50% for PPA and 30% for BENZ. The degradation dynamics of the two pollutants separately seems to happen faster than when they are mixed. It is likely that this is linked to the competition of pollutants on the active sites of photocatalyst [34].

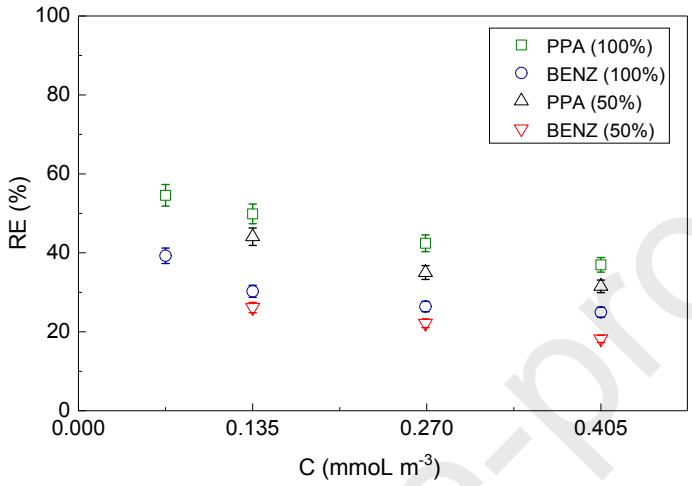

Figure 7. Photocatalytic RE of PPA alone, BENZ alone and their mixture (PPA + BENZ). Q= 2 m^3 h^{-1}, RH = 50%, I= 20 W m^{-2}, T = 20 °C. Error bars: SD (n= 5%)

3.4.2. Combined processes (NTP/SiO_2-TiO_2+UV) for the mixture (PPA and BENZ) removal

Figure 8 shows the evolution of the RE of PPA as a function of the injected voltage at a flow rate of 2 m^3 h^{-1} and a concentration of 0.135 mmoL m^{-3}. Although the PPA concentration is low (0.135 mmoL m^{-3}), the removal efficiency did not exceed 50% with photocatalysis. With combined process, the RE reaches a value higher than 60% for a voltage equal to 9 kV. Using different experimental conditions, the same phenomena was observed. The same behavior is also observed for the BENZ degradation (see Figure 9). Coupling the two processes, a synergistic effect was observed for the degradation of each pollutant. This improvement is even more marked than the effect of the injected voltage. For a voltage of 9 kV, a gain of 5% was observed, whereas for an injected voltage of 15kV, an increase of 11% was reached. In previous studies focusing on outdoor air treatment, we reported the increase of the synergetic effect with

higher injected voltages allowing an enhancement that can reach ~20% [37-38]. However, in the present study focusing on indoor air (confined environment), we are restricted to relatively weak voltages in order to control the ozone formation by the NTP.

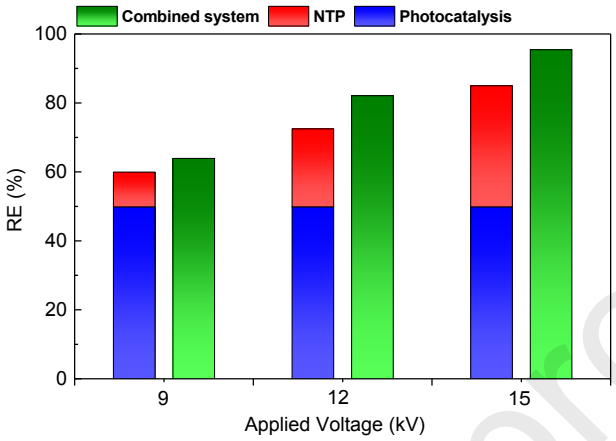

Figure 8. Removal efficiency with applied voltage using tested processes: [PPA] =0,135 mmoL m^{-3}, Q = 2 m^3 h^{-1}, RH=50%, I = 20 W m^{-2}, T = 20 °C.

This is explained by the fact that at higher voltages, the plasma of the discharge of the dielectric barrier produces a larger amount of active species ($O^{\bullet}$, $HO^{\bullet}$, $O^{\bullet}$, N, O_3, NO_2, etc…) that can enhance the pollutants oxidation performance. One of the causes of the synergistic effect is the trapping of the plasma-generated reactive species in the pores of TiO_2. At high dose of energy injected, a significant amount of these adsorbed species reduces the recombination of the photogenerated charges and thus enhances the degradation of the pollutant. It is worth to mention at this level that previous studies have shown that the UV rays created by the NTP are not sufficient to activate the photocatalyst (TiO_2) and its contribution to the improvement of the pollutant removal performance is negligible as well. The addition of external light source (UV lamp) into the plasma is essential to activate the TiO_2 photocatalyst [35,36]. Similar observations have already been reported in previous studies for the degradation of various volatile organic compounds [35-40]. The synergistic effect obtained on the surface of the photocatalyst may be due to various phenomena [41-43] such as: (i) the species generated by

the cold plasma ($O^{\bullet}$, N, O_3, NO_2, etc…) can be adsorbed on the TiO_2 in order to reduce its photo-generated charges recombination and react after with the VOC molecules at the catalyst interface leading to the improvement of the pollutant degradation [41], (ii) the plasma can enhance ions bombardment leading to improved electron/hole pairs formation at the photocatalyst interface [42], (iii) NTP can help to mineralize the by-products, which cannot be handled by photocatalysis, reducing their accumulation on the photocatalyst surface, and (iv) the decomposition of ozone under the effect of TiO_2 with UVA radiations into reactive radicals can accelerate the pollutants degradation [40,43,37]. In our previous results, we showed that when TiO_2+UVA was placed in post plasma Catalysis (PPC), a reduction of outlet ozone [40,38]. Figure 10 shows that similar phenomenon occurs for the mixture degradation.

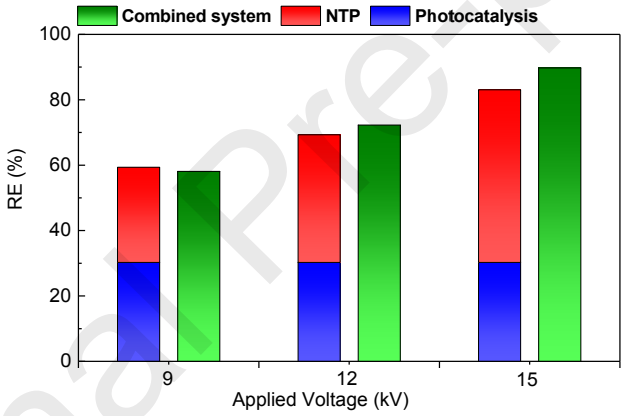

Figure 9. Removal efficiency with applied voltage using tested processes: [BENZ] =0,135 mmoL m^{-3}, Q = 2 m^3 h^{-1}, RH=50%, I = 20 W m^{-2}, T = 20 °C.

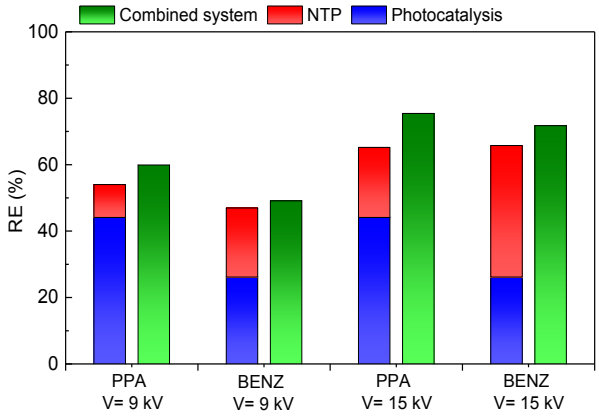

Figure 10. Removal efficiency with applied voltage using tested processes: [PPA+BENZ] =0,135 mmoL m^{-3}, Q = 2 m^3 h^{-1}, RH=50%, I = 20 W m^{-2}, T = 20 °C.

3.5. CO and CO_2 Selectivity and Ozone formation

3.5.1. Selectivity of CO_2 with photocatalytic oxidation

Figure 11 shows the selectivity of CO and CO_2 during the oxidation of PPA and BENZ under single or mixture system with the tested treatment processes (NTP, photocatalysis and NTP + photocatalysis). The results show that carbon dioxide (CO_2) is the most predominant by-product. It is clear also that the increase in the initial concentration generates a significant decrease in CO_2 selectivity. As the amount of pollutant increases, the amount of the photo-generated reactive species remains constant. Only a small fraction of the PPA and BENZ is mineralized, which corresponds to the formation of CO_2.The best selectivity in CO_2 is clearly visible at a low concentration. At low input concentrations, not all active sites are occupied, the intermediates by-products can be more easily degraded to the ultimate stage i.e. CO_2. Then, there is a competition phenomenon that takes place between PPA and BENZ and their by-products. This competition depends on the respective concentrations of each entity and the affinity of the compounds towards the catalytic support [37-38]. Globally, we note that the selectivity decreases during the mixture degradation experiment. By-products formation is more important and thus the competition phenomenon leads to less selectivity.

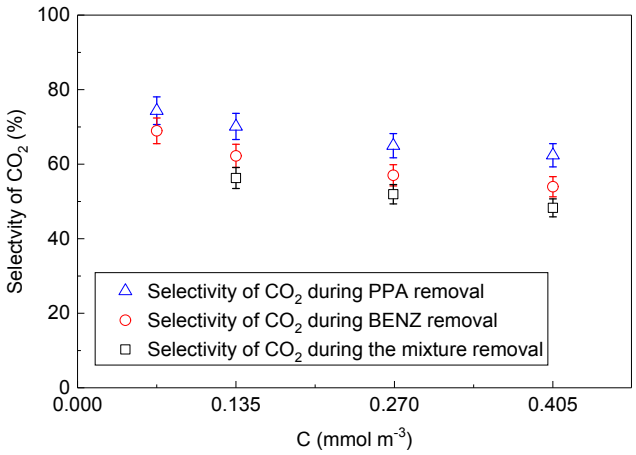

Figure 11. Comparison of CO_2 selectivity (PPA alone, BENZ alone and (PPA+BENZ) vs concentration of pollutant by photocatalysis: Q= 2 m^3 h^{-1}, I= 20 W m^{-2}. Error bars: SD (n= 5%).

3.5.2. CO and CO_2 selectivity with NTP/ TiO_2 + UV oxidation: effect of the generated O_3,

Figure 12 shows the variation of CO_x selectivity (%) and ozone (ppm) during treatment by the processes. The results of the mineralization of benzene by the three processes show that the CO selectivity is low and its value does not exceed 13%. The CO_2 selectivity during photocatalysis is higher compared to the other processes. The photocatalytic mineralization of the pollutant reached 61%, whereas the NTP alone and the NTP/SiO_2-TiO_2-UV coupling showed 35% and 43%, respectively. Ozone formation was also monitored during the NTP/SiO_2-TiO_2-UV coupling in the presence of the mixture (BENZ+PPA) as shown in Figure 12. It is worth to note that the combination of the two processes (NTP/SiO_2-TiO_2-UV) achieved a higher conversion rate of the pollutants and offered a great potential in ozone reduction compared to that obtained during the application of NTP alone. Actually, when plasma is taken alone at 15 kV, the ozone concentration is about 20 ppm. By combining the two processes, the ozone concentration decreases to 9 ppm. This behavior suggests that the used light (UVA lamps) may play an important role in oxygen decomposition as described in Equations (5 and 6) [43,44]:

$$O_3 + e^- \rightarrow O^{\bullet -} + O_2 \qquad \text{Eq.5}$$

$$O_3 + hv(\lambda < 360nm) \rightarrow O_2 + O^{\bullet} \quad \text{Eq.6}$$

Moreover, the presence of the photocatalytic material in the discharge zone reduces considerably the concentration of ozone. The photo-generation of reactive oxygen species (ROS) at the surface of the catalyst and the presence of the ozone (NTP) would also explain the synergistic effect in the conversion of VOCs [42]. Another hypothesis suggests a decrease in the source that forms ozone, that is, atomic oxygen in the plasma phase. Indeed, during the processes coupling, the RE being higher, this would mean an increasing consumption of ROS such as atomic oxygen and so redution in the ozone formation as previously reported [45].

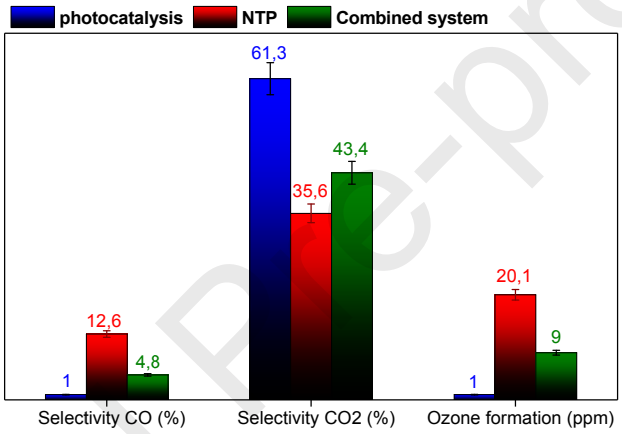

Figure 12. Variation of CO_x selectivities (%) and amount of ozone (ppm) with photocatalysis, NTP and NTP/SiO_2-TiO_2-UV. [Mixture] = 0.135 mmoL m^{-3}, Q = 2 m^3 h^{-1}, voltage = 15 kV, HR = 50%.

At this level, it is worth to illustrate the contribution of the photo-generated electron/hole for the oxidation/reduction reactions involved in the PPA degradation. This does not involve only the direct interactions between the PPA and the h^+, but also the interactions with the photo-generated species such as $^{\bullet}$OH-radical as shown in equations 7-9 below (Eq.7-9). A hydro-peroxide radical is formed (Eq. 10). This radical will react with the ethyl radical resulting from Eq. 9 leading to the formation of instable CH_3CH_2OOH molecules (Eq.11). CH_3CH_2OOH will then decompose into alcohol and aldehyde (Eq. 12 and 13). These latter compounds will then

decompose into CO_2. It is important to mention that more H_2O is formed during the degradation pathway; more it is complex to control/identify the intermediate compounds.

$$CH_3CH_2COOH + h^+ \rightarrow CH_3CH_2^{\bullet} + CO_2 + H^+ \quad (7)$$

$$H_2O + h^+ \rightarrow {}^{\bullet}OH + H^+ \quad (8)$$

$$CH_3CH_2COOH + {}^{\bullet}OH \rightarrow CH_3CH_2^{\bullet} + CO_2 + H_2O \quad (9)$$

$$O_2 + e^- + H^+ \rightarrow HO_2 \quad (10)$$

$$CH_3CH_2^{\bullet} + HO_2^{\bullet} \rightarrow CH_3CH_2OOH \quad (11)$$

$$CH_3CH_2OOH \rightarrow CH_3CH_2OH + \tfrac{1}{2}\, O_2 \quad (12)$$

$$CH_3CH_2OOH \rightarrow CH_3CHO + H_2O \quad (13)$$

This mechanism is in agreement with the one drawn by Kraeutler and Bard [46] on the degradation of deuterated acrylic acid. Kraeutler and Bard showed that the H-atoms resulting from the carboxylic groups led to the formation of Alkane molecules.

3.6. Poisoning and regeneration of the photocatalyst

3.6.1. Catalyst poisoning

The efficiency of the combined processes has been proven to removal organic compounds in terms of degradation and mineralization. Synergism between photocatalysis and NTP was observed in both cases of PPA and BENZ degradation. It was also observed for the mixture (PPA+BENZ) degradation. In order to better understand the catalyst lifetime and the synergistic effect during BENZ removal, experiments with complementary mixtures were carried out. First, the study of photocatalytic poisoning during a long-term photocatalytic treatment is discussed. Then, the study of the catalyst regeneration and its reuse is investigated.

The evolution of the removal of BENZ contained in BENZ+PPA mixture during 7 h of the photocatalytic oxidation treatment is presented in Figure 13. The experiment was carried out under low humidity conditions (5 % RH). A mixture of the gaseous effluent (50% PPA-50% BENZ) is injected in the cylindrical reactor at a flow rate of 2 m^3 h^{-1} and a concentration of 0.54 mmoL m^{-3}. A decrease in the effectiveness of the degradation of BENZ is reported after 7 hours of photocatalytic treatment under UV radiation. At the beginning of the experiment (t = 5min), the initial value of the abatement is ~29%. This decrease in the performance of the photocatalytic process can be attributed to the accumulation of by-products during several cycles of treatment on the active sites of the catalyst. This generates a progressive deactivation of SiO_2-TiO_2-GFT catalyst, which results in the decrease of the pollutant removal and the operational lifetime of the catalyst.

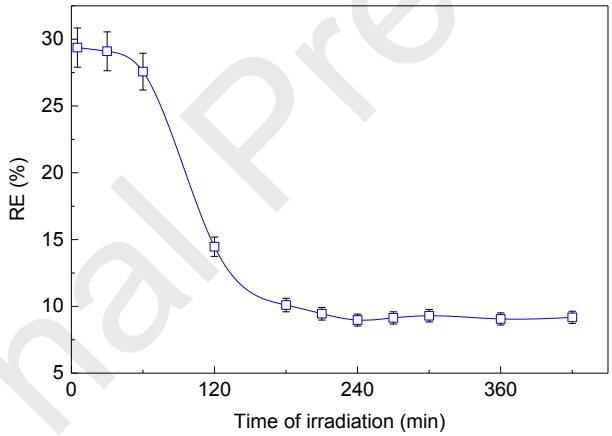

Fig.13. Evolution of the removal of BENZ from the mixture (PPA + BENZ) by the photocatalytic process (SiO_2-TiO_2-UV). [Mixture] = 0.54 mmoL m^{-3}, Q = 2m^3 h^{-1}, RH= 5%, T = 20 °C.

3.6.2. Regeneration and reuse of SiO_2-TiO_2-GFT catalyst

After showing that the photocatalyst is poisoned during the long-term process, it is necessary to regenerate it and to follow if it can recover its effectiveness. Thus, this part is devoted to studying the possibility of restoring the initial performance of the photocatalyst. The application

of NTP in the absence of UV radiation at 2 $m^3 h^{-1}$ is shown to regenerate the photocatalyst. This experiment was carried out without injecting the pollutant into air feed. Two NTP regeneration periods were tested, 30 min and 3 h. Three photocatalytic cycles were carried out successively on the same catalyst. At the end of each cycle, the catalyst was reactivated for reuse in a new cycle. Figure 14 presents the evolution of the RE of BENZ during the photocatalytic treatment using NTP. The results obtained show that under these working conditions, more than 29% of the catalytic efficiency was recovered within 30 min of regeneration. The RE performance obtained by the regenerated of the catalyst by NTP for 30 min is better than those obtained after regenerating the catalyst for 3 hours. This can be attributed to the ozone accumulation on the catalyst sites during the 3h regeneration. Similar result has been previously obtained at lab-scale, which confirms the results obtained in this study [48,49,37,38]. According to Sivachandiran et al., the surface of TiO_2 charged with isopropanol was fully regenerated by NTP using a fixed bed reactor [41]. This observation was also reported by Mok et al., in their comparison between plasma regeneration and thermal regeneration of a deactivated Ni/alumina catalyst [47].

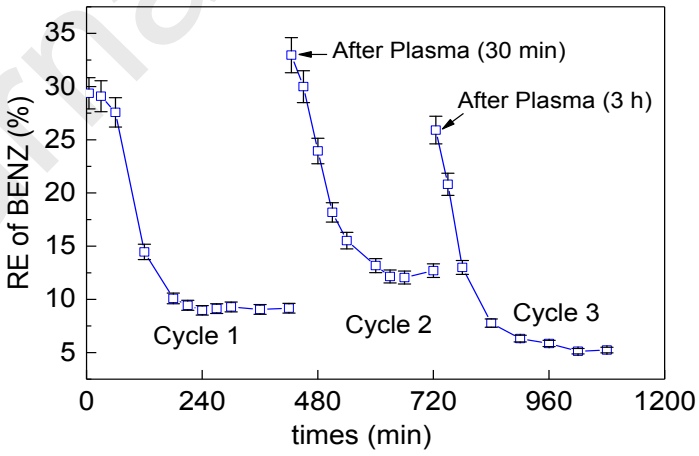

Figure 14. Evolution of removal efficiency of BENZ during the removal of PPA and BENZ mixed with photocatalysis (SiO_2-TiO_2-UV) by NTP as a regeneration method for poisoned SiO_2-TiO_2-GFT. [Mixture] = 0.54 mmoL m^{-3}, Q = 2 $m^3 h^{-1}$, RH = 5%, T = 20 ° C.

Conclusions

In this study, the elimination of PPA alone, BENZ alone and their mixture was studied for refrigerated chambers at pilot scale. The removal efficiency of PPA mixed with BENZ was studied by applying photocatalysis, NTP and the coupling of both processes (NTP/SiO_2-TiO_2-UV). Photocatalysis alone was seen to mineralize 60 % of the model VOC, however, the combined system showed 43% pollutant mineralization. In addition, we showed that the NTP coupled to SiO_2-TiO_2-UV photocatalysis improved the performance of the process in terms of pollutants degradation (but not in mineralization). The removal efficiency of PPA with BENZ and the selectivity to CO_2 were improved and the amount of ozone at the outlet of the reactor was reduced. CO did not exceed 13%. Considering the toxicity of this molecule, this selectivity value is far below the accepted values for the quality of indoor air. The reduction of the pollutants by photocatalytic treatment was strongly influenced by the air flow, the initial concentration(s) of the pollutant(s) and the relative humidity. The increase of these two operating parameters led to a decrease in the RE. It has been shown that for the NTP, the efficiency of the removal of the pollutants is highly dependent on the applied voltage. The study disclosed also on the performances of the NTP in-situ regeneration of the catalyst. Regeneration by NTP enhanced the pollutants desorption, the ozone formation and the degradation intermediates that can accumulated on the catalytic active sites. This study introduces possible industrial applications of these combined processes for food industry and other production chains that suffer from malodors.

References

[1] S. Camille, F. Xavier, La pollution olfactive en environnement urbain: cas particulier des odeurs des restaurants Olfactory pollution in urban environment: special case of odors in restaurants, Pollution Atmosphérique 234 (2017) 1-20.

[2] K. Ki-Hyun, P. Shin-Young, A comparative analysis of malodor samples between direct, Atmospheric Environment 42 (2008) 5061-5070.

[3] T. Paul, D. Sree, H. Aglan, Effect of mechanically induced ventilation on the indoor air quality of building envelopes Energy Buildings 42 (2010) 326–332.

[4] M. Paulina, R. Wojciech, Odor Emission Factors from Livestock Production, Polish Journal of Environmental Studies 27 (2015) 27-35.

[5] J. Sang-Hee, K. Ki-Hyun, K. Yong-Hyun, L. Min-Hee, K. Bo-Won, A. Jeong-Hyeon, Deodorization of food-related nuisances from a refrigerator: The feasibility test of photocatalytic system, Chemical Engineering Journal 277 (2015) 260-268.

[6] W. Yu-feng, C. Jun-shui, L. Chen, F. Xu-dong, Z. Ji-dong, S. E. E. Inspection, Q. Bureau, Determination of 6 Benzene Organic Compounds in Food-grade Lubricating Oils by Headspace-gas Chromatography-mass Spectrometry. The Food Industry 11 (2015) 077.

[7] P. Bourke, D. Ziuzina, D. Boehm, P.J. Cullen, K. Keener, The potential of cold plasma for safe and sustainable food production. Trends in biotechnology 36 (2018) 615-626.

[8] K.-H. Kim, Y.-H. Kim, Composition of key offensive odorants released from fresh food materials, Atmos. Environ. 89 (2014) 443–452.

[9] S. Selena, C. Laura, C. Paolo, D. R. Renato, G. Massimiliano Il, Odour emission factors for assessment and prediction of Italian MSW landfills odour impact, Atmospheric Environment. 39 (2005) 5387-5394.

[10] P. Wilhelm, History of Odor and Odorants, Springer Handbook of Odor. (2017) 5-6.

[11] S. Wing, R.A. Horton, S.W. Marshall, K. Thu, M. Tajik, L. Schinasi, S.S. Schiffman, Air pollution and odor in communities near industrial swine operations. Environmental health perspectives. 116 (2008) 1362.

[12] S. Nimmermark, Odour influence on well-being and health with specific focus on animal production emissions. Annals of Agricultural and Environmental Medicine. sued (2004), 11

(2), pp 163. http://www.bape.gouv.qc.ca/sections/mandats/LET-Lachenaie/documents/DB69.pdf.

[13] J. CARRE, (2006) Pollution olfactive, sources d'odeurs, cadre reglementaire, techniques de mesure et procèdes de traitement. https://www.record-net.org/storage/etudes/03.../Rapport_record03-0808-0809_1A.pdf.

[14] C. Couturier, L. Galtier, P.P. Arm, H. Brugere, L. Marache, M.K. Ensat, (1998) Etat des connaissances sur le devenir des germes pathogenes et des micropolluants au cours de la methanisation des déchets et sous-produits organiques. https://solagro.org/images/imagesCK/files/publications/f33_impactsdelamethanisationsurlesgermesphatogenes.pdf.

[15] Y. Chen, X. Li, X. Zheng, D Wang, Enhancement of propionic acid fraction in volatile fatty acids produced from sludge fermentation by the use of food waste and Propionibacterium acidipropionici. Water research. 47 (2013) 615-622.

[16] Priority Pollutants. Code of Federal Regulations, (1996) Title 40; U.S. Environmental Protection Agency, U.S. Government Printing Office: Washington, DC, (Chapter 1, Part 423, Appendix A).

[17] H. Ren, P. Koshy, W.F. Chen, S. Qi, C.C.Sorrell, Photocatalytic materials and technologies for air purification, Journal of Hazardous Materials. 325 (2017) 340–366.

[18] N. Novak Tušar, A. Šuligoj, U. Lavrenčič Štangar, TiO_2/SiO_2 films for removal of Volatile Organic Compounds (VOCs) from indoor air, Chapter 25 in Handbook of Ecomaterials 1, pp. 589-605 (2019) Springer-Nature, ISBN: 978-3-319-68256-3.

[19] M. Q. Wen, T. Xiong, Z. G. Zang, W. Wei, X. S. Tang, and F. Dong, Synthesis of MoS_2/g-C_3N_4 nanocomposites with enhanced visible-light photocatalytic activity for the removal of nitric oxide (NO) 4 (2016) 10205-10212.

[20] V.K. Yemmireddy, Y.C. Hung, Using photocatalyst metal oxides as antimicrobial surface coatings to ensure food safety—opportunities and challenges. Comprehensive Reviews in Food Science and Food Safety. 16 (2017) 617-631.

[21] A. A. Assadi, A. Bouzaza, D. Wolbert, P. Petit, Isovaleraldehyde elimination by UV/TiO_2 photocatalysis: comparative study of the process at different reactors configurations and scales, Environmental Science and Pollution Research 21 (2014) 11178-11188.

[22] Z. Jiang, M. Chen, J. Shi, J. Yuan, W. Shangguan, Catalysis Removal of Indoor Volatile Organic Compounds in Room Temperature: From Photocatalysis to Active Species Assistance Catalysis. Catal. Surv. Asia. 19 (2015) 1-16.

[23] U.I. Gaya, A.H. Abdullah, Heterogeneous photocatalytic degradation of organic contaminants over titanium dioxide: A review of fundamentals, progress and problems.Journal of Photochemistry and Photobiology C: Photochemistry 9 (2008) 1-12.

[24] A.A. Assadi, A. Bouzaza, C. Vallet, D. Wolbert, Use of DBD plasma, photocatalysis and combined DBD plasma/photocatalysis in a continuous annular reactor for isovaleraldehyde elimination: Synergetic effect and byproducts identification. Chem. Eng. J. 254 (2014) 124-132.

[25] Ahlstrom Patent EP 1069950, 2000. AU 735798 US 09/467, 650; JP 2000-542104.

[26] T. Zadi, A.A. Assadi, N. Nasrallah, R. Bouallouche, P.N. Tri, A. Bouzaza, M.M. Azizi, R. Maachi, D. Wolbert, Treatment of hospital indoor air by a hybrid system of combined plasma with photocatalysis: Case of trichloromethane, Chemical Engineering Journal 349 (2018) 276-286.

[27] J. Rodier, (1996). The Analysis of Water: Natural Water. Wastewater, Sea Water: Physical.

[28] A.A. Assadi, J. Palau, A. Bouzaza, D. Wolbert A., Modeling of a continuous photocatalytic reactor for isovaleraldehyde oxidation: Effect of different operating parameters and chemical degradation pathway- Chem Eng Res Des. 91(2013) 1307–1316.

[29] S.B. Kim, S.C. Hong, Kinetic study for photocatalytic degradation of volatile organic compounds in air using thin film of a TiO_2 photocatalyst, Appl. Catal. B. 35 (2002) 305–315.

[30] J. Palau, A.A. Assadi, J.M. Penya-roja, A. Bouzaza, D. Wolbert, V. Martínez-Soria, Isovaleraldehyde degradation using UV photocatalytic and dielectric barrier discharge reactors, and their combinations, J. Photochem.Photobiol. A Chem. 299 (2015) 110–117.

[31] T. Ochiai, A. Fujishima, Photoelectrochemical properties of TiO_2 photocatalyst and its applications forenvironmental purification, Journal of Photochemistry and Photobiology C: Photochemistry Reviews. 13 (2012) 247–262.

[32] A. A. Assadi, A. Bouzaza, D. Wolbert, Study of synergetic effect by surface discharge plasma/TiO_2 combination for indoor air treatment: Sequential and continuous configurations at pilot scale, Journal of Photochemistry and Photobiology A: Chemistry 310 (2015) 148-154.

[33] S. Lu, L. Chen, Q. Huang, L. Yang, C. Du, X. Li, J.Yan, Decomposition of ammoniaand hydrogen sulfide in simulated sludge drying waste gas by a novel non-thermal plasma. Chemosphere 117 (2014) 781-785.

[34] O. Debono, V. Hequet, L. Le Coq, N. Locoge, F. Thevenet, VOC ternary mixture effect on ppb level photocatalytic oxidation: Removal kinetic, reaction intermediates and mineralization, Appl. Catal. B: Environ. 218 (2017) 359-369.

[35] F. Thevenet, O. Guaitella, E. Puzenat, J.M. Herrmann, A. Rousseau, C. Guillard, Oxidation of acetylene by photocatalysis coupled with dielectric barrier discharge. Catal.Today. 122 (2007) 186-194.

[36] A.A. Assadi, J. Palau, A. Bouzaza, J. Penya-Roja, V. Martinez-Soriac, D. Wolbert, Abatement of 3-methylbutanal and trimethylamine with combined plasma and

photocatalysis in a continuous planar reactor. J. Photochem. Photobiol. A Chem. 282 (2014) 1-8.

[37] W. Abou Saoud, A. A. Assadi, M. Guiza, A. Bouzaza, W. Aboussaoud, I. Soutrel, A. Ouederni, D. Wolbert, S. Rtimi, Abatement of ammonia and butyraldehyde under non-thermal plasma and photocatalysis: Oxidation processes for the removal of mixture pollutants at pilot scale, Chemical Engineering Journal 344 (2018) 165-172

[38] W. Abou Saoud, A. A. Assadi, M. Guiza, S. Loganathan, A. Bouzaza, W. Aboussaoud, A. Ouederni, S. Rtimi, D. Wolbert, Synergism between non-thermal plasma and photocatalysis: Implications in the post discharge of ozone at a pilot scale in a catalytic fixed-bed reactor. Applied Catalysis B: Environmental 241 (2019) 227-235.

[39] A. Maciuca, C. Batiot-Dupeyrat, J.M. Tatibouët, Synergetic effect by coupling photocatalysis with plasma for low VOCs concentration removal from air. Appl. Catal.B Environ. 125 (2012) 432-438.

[40] S. Abou Ghaida, A.A. Assadi, G. Costa, A. Bouzaza, D. Wolbert, Association of surface dielectric barrier discharge and photocatalysis in continuous reactor at pilot scale: Butyraldehyde oxidation, by-products identification and ozone valorization. Chemical Engineering Journal 292 (2016) 276-283.

[41] L. Sivachandiran, F. Thevenet, P. Gravejat, A, Rousseau, Isopropanol saturated TiO_2 surface regeneration by non-thermal plasma: influence of air relative humidity. Chemical Engineering Journal 214 (2013)17-26.

[42] A.M. Vandenbroucke, R. Morent, N.D. Geyter, C. Leys, Non-thermal plasmas for non-catalytic and catalytic VOC abatement, Review. J. Hazard. Mater. 195 (2011) 30-54.

[43] J. Taranto, D. Frochot, P. Pichat, Combining cold plasma and TiO_2 photocatalysis to purify gaseous effluents: a preliminary study using methanol-contaminated air. Ind. Eng. Chem. Res. 46 (2007) 7611-7614.

[44] H. Huang, D. Yea, Combination of photocatalysis downstream the non-thermal plasma reactor for oxidation of gas-phase toluene. J. Hazard. Mater. 171 (2009) 535-541.

[45] S. Futamura, H. Einaga, H. Kabashima, Y.H. lee, Synergistic effect of silent discharge plasma and catalysts on benzene decomposition. Catal. Today 89 (2004) 89-95.

[46] B. Kraeutler, and A. J. Bard, Heterogeneous photocatalytic decomposition of saturated carboxylic acids on titanium dioxide powder. Decarboxylative route to alkanes, J. Am. Chem. Soc. 100 (1978) 5985–5992.

[47] Y.S. Mok, E. Jwa, Y.J. Hyun, Regeneration of C4H10 dry reforming catalyst by nonthermal plasma. J. Energy Chem. 22 (2013) 394-402.

[48] W. Abou Saoud, A. A. Assadi, M. Guiza, A. Bouzaza, W. Aboussaoud, A. Ouederni, I. Soutrel, D. Wolbert, S. Rtimi, Study of synergetic effect, catalytic poisoning and regeneration using dielectric barrier discharge and photocatalysis in a continuous reactor: Abatement of pollutants in air mixture system. Applied Catalysis B: Environmental 213 (2017) 53-61

[49] W. Elfalleh, A.A. Assadi, A. Bouzaza, D. Wolbert, J. Kiwi, S. Rtimi, Innovative and stable TiO_2 supported catalytic surfaces removing aldehydes under UV-light irradiation. Journal of Photochemistry and Photobiology A: Chemistry 343 (2017) 96-102.

Declaration of interests

☒ The authors declare that they have no known competing financial interests or personal relationships that could have appeared to influence the work reported in this paper.

☐The authors declare the following financial interests/personal relationships which may be considered as potential competing interests:

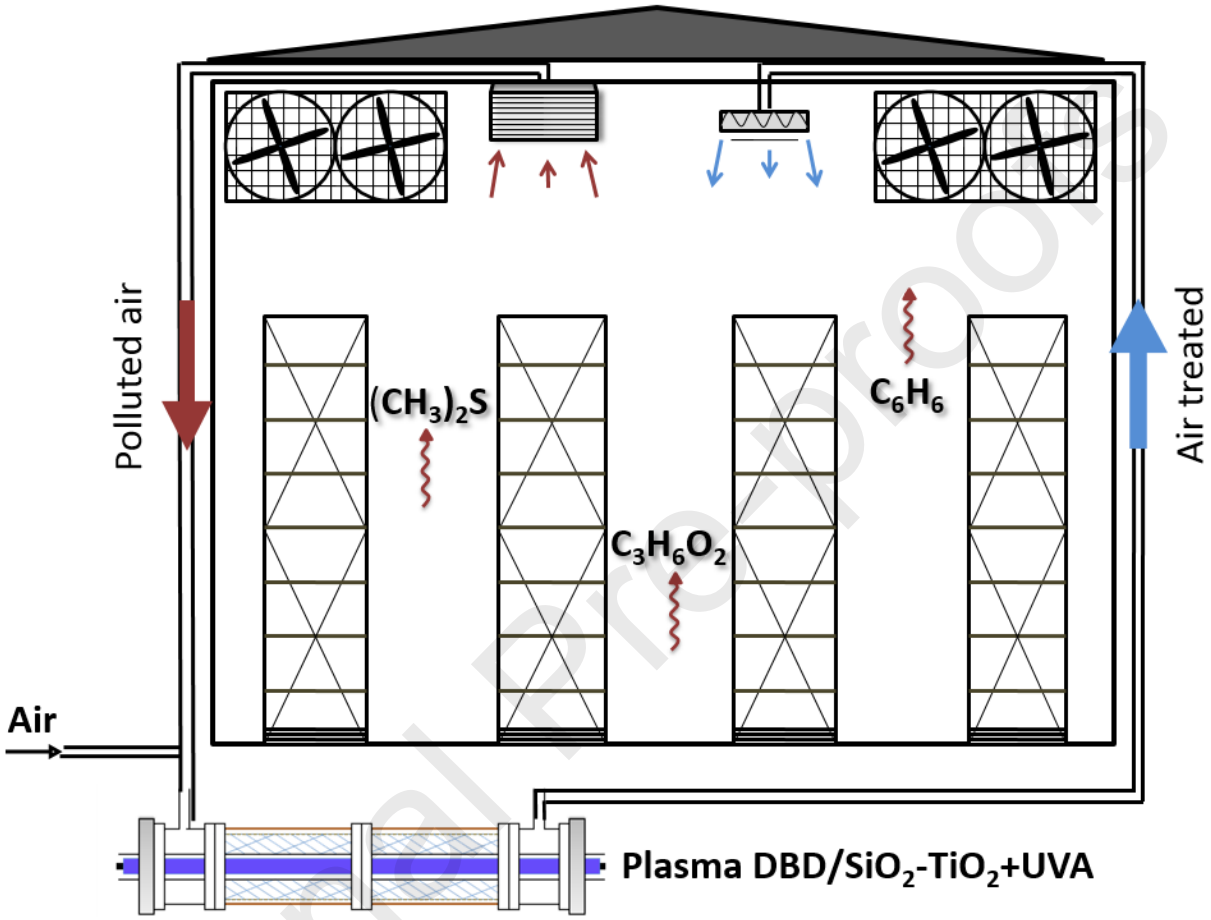

A hybrid system combining plasma with photocatalysis for treatment of refrigerated food chambers.

Highlights:

- A possible way for treat of air from refrigerated food chambers is proposed.
- Non-Thermal Plasma was coupled to Photocatalysis for indoor air treatment
- The impact of the operating parameters on performance of the process are tested.
- The removal of Propionic Acid and Benzene each alone and in mixture are studied.
- Poisoning and catalyst regeneration capacity with non-thermal plasma is studied.